J Solid State Electrochem (2007) 11:1211–1219
DOI 10.1007/s10008-007-0272-x

ORIGINAL PAPER

Characterization of gold nanoparticles electrochemically deposited on amine-functioned mesoporous silica films and electrocatalytic oxidation of glucose

Jing-Jing Yu · Shuang Lu · Jiang-Wen Li · Fa-Qiong Zhao · Bai-Zhao Zeng

Received: 8 October 2006 / Revised: 4 January 2007 / Accepted: 8 January 2007 / Published online: 7 February 2007

Abstract This study reports the preparation and characterization of gold nanoparticles deposited on amine-functioned hexagonal mesoporous silica (NH_2–HSM) films and the electrocatalytic oxidation of glucose. Gold nanoparticles are fabricated by electrochemically reducing chloroauric acid on the surface of NH_2–HSM film, using potential step technology. The gold nanoparticles deposited have an average diameter of 80 nm and show high electroactivity. Prussian blue film can form easily on them while cycling the potential between −0.2 and 0.6 V (vs saturated calomel electrode) in single ferricyanide solution. The gold nanoparticles loading NH_2–HSM-film-coated glassy carbon electrode (Au–NH_2–HSM/GCE) shows strong catalysis to the oxidation of glucose, and according to the cathodic oxidation peak at about 0.16 V, the catalytic current is about 2.5 μA mM^{-1}. Under optimized conditions, the peak current of the cathodic oxidation peak is linear to the concentration of glucose in the range of 0.2 to 70 mM. The detection limit is estimated to be 0.1 mM. In addition, some electrochemical parameters about glucose oxidation are estimated.

Keywords Gold nanoparticles · Mesoporous silica · Prussian blue · Glucose · Voltammetry

Introduction

Highly dispersed gold nanoparticles has been demonstrated to be very active catalyst for a number of important chemical reactions [1–4]. It has also been widely used in the fabrication of modified electrodes and biosensors, as it has excellent biological compatibility as well as large surface area [5, 6]. Various methods have been used to prepare gold nanoparticles, such as thermal hydrogen reduction, photoreduction, and electrochemical reduction of gold precursors in solution or on the surface of metal oxides and polymers [7, 8]. However, to precisely control the size and morphology of nanoparticles is still a challenging work.

Recently, mesoporous materials attracted an increasing interest in nanoparticles preparation. Mesoporous materials possess uniform void spaces; researchers thought that they could serve as templates for forming nanoparticles. In particular, several kinds of mesoporous silica can be synthesized on a large scale and are commercially available, such as hexagonal mesoporous silica (HSM), mesoporous molecular sieve (MCM-41), and SBA-15. They have a two-dimensional pore structure with a channel diameter of less than 10 nm and a high surface area of up to 1,000 m^2 g^{-1} [9]. In such pore structure, metal particles can interact with each other only in the same pore; between neighboring pores, no interaction occurs [10]. Nanoparticles deposited on those materials are confined in the pores, so they have controlled size and high dispersion. Gold nanoparticles have been prepared by using mesoporous materials as template via three routes. The first involves the impregnation of gold salts in the pores of mesoporous materials and subsequent reduction (e.g., hydrogen reduction [10–12], electrochemical reduction [13], and self-reduction after thiol-function [14]) or reaction with appropriate reagents to produce metal nanoparticles [15]. Another method is to introduce gold salts in the synthesis pot of mesoporous materials before reaction, followed by chemical reduction or thermal treatment, leading to the formation of nanoparticles inside the pores or on the walls of the materials [16]. The third way is to encapsulate premade nanoparticles during the synthesis of mesoporous

J.-J. Yu · S. Lu · J.-W. Li · F.-Q. Zhao · B.-Z. Zeng (✉)
Department of Chemistry,
Wuhan University,
Wuhan 430072, People's Republic of China
e-mail: bzzeng@whu.edu.cn

materials [17]. As mentioned above, electrochemical technology is also adopted in the fabrication of gold nanoparticles on mesoporous material. For example, Pérez et al. [13] prepared gold nanoparticles on mesoporous TiO_2 through electrochemical deposition, in which the mesoporous film-coated electrode was immersed in a 5×10^{-5} M chloroauric acid for 10 h to allow gold ions to diffuse into the pores, followed by an electrochemical deposition of 120 min. Compared with other methods, the electrochemical method generally has two advantages. One is the high purity of metal nanoparticles obtained; another is the controllability of particle size by adjusting the current density or applied potential [18].

In this article, gold nanoparticles are fabricated by electrochemical technology on amine-functioned mesoporous silica. Before electrochemical deposition, the mesoporous material film-coated electrode is immersed into a chloroauric acid aqueous solution. Owing to electrostatic attraction, it only needs 30 min for chloroauric ions to achieve a saturated adsorption. The resulted gold nanoparticle-coated electrode is characterized by scanning electron microscopy (SEM), transmission electron microscopy (TEM), and electrochemical method. The gold nanoparticles shows high electroactivity. A Prussian blue (PB) film can form on it from a single ferricyanide solution and exhibit well-defined voltammetric peaks. The electrode shows strong catalysis to glucose oxidation.

Experimental

Chemicals

Aminopropyltrimethoxysilane (APTES) and mercaptopropyltrimethoxysilane (MPTMS) were purchased from Silicone Material Co. of Wuhan University and Aldrich, respectively. Mesoporous silica HSM was synthesized according to [19], in which cetanedecylamine was used as template. The pore diameter of the HSM was estimated to be 4 nm according to the adsorption and desorption of nitrogen gas. Polyvinyl alcohol (PVA; average degree of polymerization, 1,750±50) came from Sinopharm Chemical Reagent (Shanghai, China). The other chemicals used were of analytical grade, and the solutions were prepared with double-distilled water.

Apparatus

All voltammetric experiments were performed on a CHI 660A electrochemical analyzer (Chenhua Instruments, Shanghai, China). The working electrode was a modified glassy carbon electrode (GCE) with a geometric area of 0.033 cm^2. A saturated calomel electrode (SCE) served as the reference electrode, and a Pt wire as the counter electrode. The measurement of electrochemical impedance spectroscopy (EIS) was carried out with an EG&G model 283 electrochemical workstation and an EG&G model 5210 lock-in amplifier (Princeton Applied Research) powered by the Powersuit software. In EIS, the frequency range was from 100 mHz to 100 kHz with an amplitude of 5 mV, and the direct current (DC) potential was the average peak potential (vs the SCE) of the oxidation and the reduction peaks. The infrared spectra were obtained using Nicolet FTIR-360 spectrometer (USA). The SEM and TEM images were obtained using a Quanta 200 SEM (FEI, Holand) and a JEM-100CXII (Japan), respectively. Before recording the TEM images, the amine-functioned mesoporous silica film with gold deposit was scraped from the electrode and then dispersed in ethanol with the aid of ultrasonic agitation. The adsorption and desorption experiments of nitrogen gas were performed on an ASAP 2020M instrument (Micromeritics, USA).

Functionalization of mesoporous silica

Before functionalization, the mesoporous silica was dehydrated at 423 K in a vacuum [20]. Then, 1-g pure silica HSM was dispersed in 50-ml dry toluene with the aid of stirring at room temperature. The organosilane (i.e., 15-ml APTES or 6-ml MPTMS) was slowly added to the mixture and allowed to react in nitrogen gas circumstance for 6 h (for APTES) or 24 h (for MPTES) in a refluxing system. The functionalized products were separated from the solution by centrifugation, washed for several times with toluene followed by ethanol, and then dried at 100 °C [21]. The products were labeled as NH_2–HSM or SH–HSM.

Preparation of gold nanoparticles loading mesoporous film-coated electrode

A 3-mg NH_2–HSM was dispersed in 1-ml dimethylformamide with the aid of ultrasonic agitation. Then, 20 μl of 3% PVA aqueous solution was added to 100-μl NH_2–HSM suspension, followed by ultrasonic agitating. Before modification, the bare GCE was polished until mirror smooth with 0.05-μm Al_2O_3 slurry, rinsed with water, then ultrasonicated in water and ethanol for several minutes. After that, 5 μl of the resulting suspension was transferred onto the GCE surface, and the solvent was evaporated under room temperature. The modified electrode was noted as NH_2–HSM/GCE. For comparison, a SH–HSM-film-coated electrode (SH–HSM/GCE), HSM-film-coated electrode (HSM/GCE), and PVA-film-coated electrode (PVA/GCE) were prepared through a similar way.

Gold nanoparticles were deposited from 4-mg ml^{-1} $HAuCl_4$ aqueous solution by electrochemical method. Before deposition, the NH_2–HSM/GCE was immersed in the solution for a certain time to allow chloroauric acid ion

to diffuse into the pores. Subsequently, the potential was adjusted to 0.80 V, and stepwise decreased to 0.65 V [13]. After 80 cycles of potential step, the electrode underwent successive cyclic potential scan in a 0.5-M H_2SO_4 solution until a stable voltammogram was obtained. The resulting modified electrode was labeled as Au–NH_2–HSM/GCE. Au–SH–HSM/GCE and Au–HSM/GCE were prepared using a similar method.

Results and discussion

Infrared spectra of functioned mesoporous silica

Figure 1 shows the infrared spectra of functionalized HSM. For NH_2–HSM, the absorption band at 3,442 cm^{-1} is assigned to the stretching vibration of isolated Si–OH. The absorption bands at 1,087, 795, and 465 $cm^{-1}$are the characteristic absorption of Si–O–Si that are assigned to asymmetric stretching, symmetric stretching, and bend vibrations, respectively. The absorption bands at 2,928, 1,632, 1,384 cm^{-1} are assigned to C–H asymmetric stretching, NH_2 scissor, CH_3 bending vibrations, respectively. The spectrum is similar to those reported in literature [22, 23]. The presence of $–CH_3$ bending vibration bands suggests a small amount of $–OCH_3$ remain. For SH–HSM, the assignment of absorption bands of 3,430, 2,929, 1,384, 1,090, 803, 468 cm^{-1} is the same as those of NH_2–HSM. The band at 1,635 cm^{-1} is assigned to C–S scissor. This suggests that the amine group and thiol group be grafted on the HSM successfully.

Deposition of gold nanoparticles

When cyclic voltammetry and constant potential electrolysis are adopted, the gold deposited on the NH_2–HSM/GCE is golden and thick, indicating that the deposited particles are quite big or that the gold films occur. However, when potential step technology is employed, the situation is different. Herein, the NH_2–HSM/GCE is immersed in a 4-mg ml^{-1} $HAuCl_4$ aqueous solution for 30 min to allow chloroauric acid ions diffusing into the pores; then, let the potential step from 0.80 to 0.65 V for 80 cycles, and the width of the potential step is 0.25 s. As a result, the NH_2–HSM/GCE becomes red-bluish. The SEM image proves that the gold particles deposited are nanoparticles (Fig. 2).

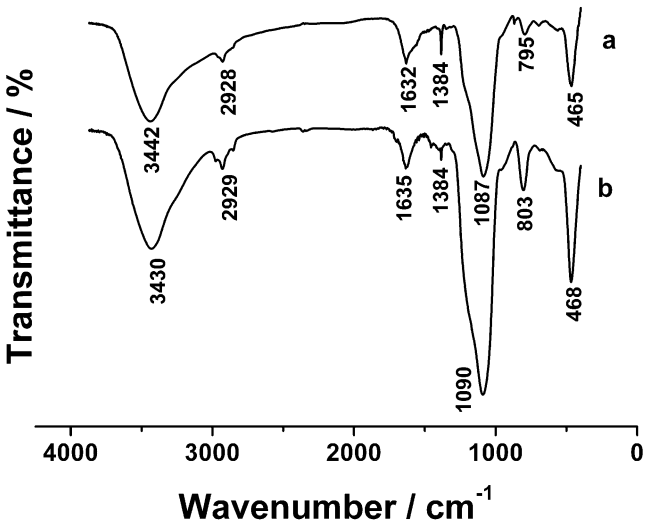

Fig. 1 IR spectra of NH_2–HSM (**a**) and SH–HSM (**b**)

As the resulted Au–NH_2–HSM/GCE exhibits bigger cathodic peak in 0.5-M H_2SO_4 solution than Au–HSM/GCE and Au–SH–HSM/GCE (Fig. 3), it can be thought that NH_2–HSM has better promotion to gold nanoparticles deposition. This should be ascribed to the influence of amine group. Under acidic condition, the amine group turns to $-NH_3^+$ and can attract electrostatically $AuCl_4^-$, enhancing the adsorption of $AuCl_4^-$ on the mesoporous silica. Therefore, more gold nanoparticles form on NH_2–HSM/GCE than on other two electrodes. Furthermore, an amine group could stabilize nanoparticles [14].

The immersing time of NH_2–HSM/GCE in $HAuCl_4$ aqueous solution influences the amount of gold nanoparticles deposited (Fig. 4). Without immersing, almost no gold nanoparticles are observed on the mesoporous film-coated electrode. In the first 30 min, the coverage of gold nanoparticles increases rapidly and then slows down. This is related to the saturated adsorption of chloroauric acid ion on the NH_2–HSM surface. The immersing time is 30 min in the following experiments.

In addition, it is found that the amount of gold nanoparticles deposited change slightly when the potential step cycle increases from 20 to 300 times. Gold nanoparticles can also be obtained when NH_2–HSM/GCE is transferred to H_2SO_4 solution for electrochemical deposition after being immersed in $HAuCl_4$ aqueous solution for some time. This indicates that the gold nanoparticles deposited mainly result from the reduction of the adsorbed or entrapped $AuCl_4^-$ in this case. Herein, 80 cycles of potential step is adopted.

SEM and TEM images of gold nanoparticles

As shown in Fig. 2, many particles are visible on the NH_2–HSM surface after the deposition of gold nanoparticles. According to the SEM image (Fig. 2b) and TEM image (Fig. 2c), the gold nanoparticles are not uniform, and their average diameter is estimated to be 80 nm. Some gold nanoparticles seem to separate from the matrix of mesoporous silica and aggregate together (Fig. 2c), which results from the ultrasonic agitation during the pretreatment process. The diameter of HSM is only 4 nm as mentioned previously, and it is much smaller than that of the gold

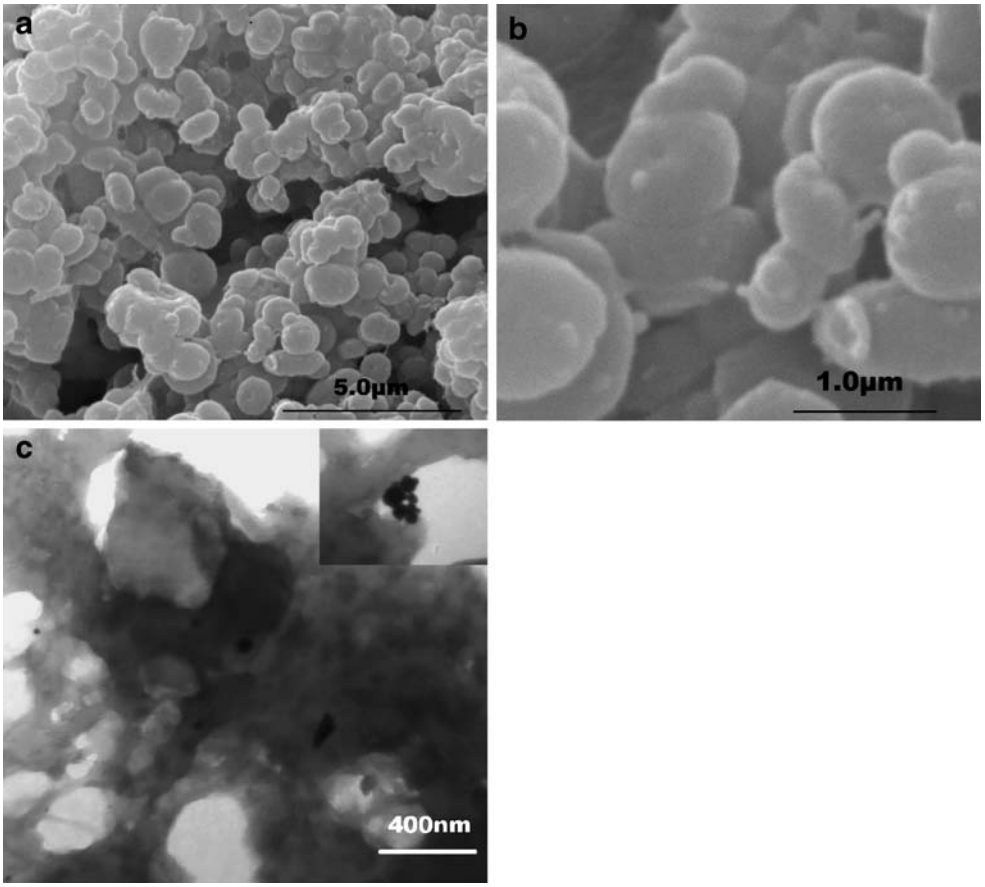

Fig. 2 SEM (**a**, **b**) and TEM (**c**) images of gold nanoparticles deposited on NH_2–HSM film. The inset of **c** shows TEM image located in different points with the same scale as **c**

nanoparticles. It indicates that the gold nanoparticles must grow in and outside the pores and then form bigger particles. This can be interpreted as follows [10]: On one hand, owing to the higher surface energy and migration of nanoparticles, the smaller particles tend to combine together and become bigger particles; on the other hand, the emission and transfer of adatoms from small particles to bigger particles also makes the particles become larger.

Electrochemical characterization of mesoporous film-coated electrodes

Voltammograms of Au–NH_2–HSM/GCE in H_2SO_4

Figure 5 shows the cyclic voltammograms (CV) of Au–NH_2–HSM/GCE in H_2SO_4 just after loading gold nano-

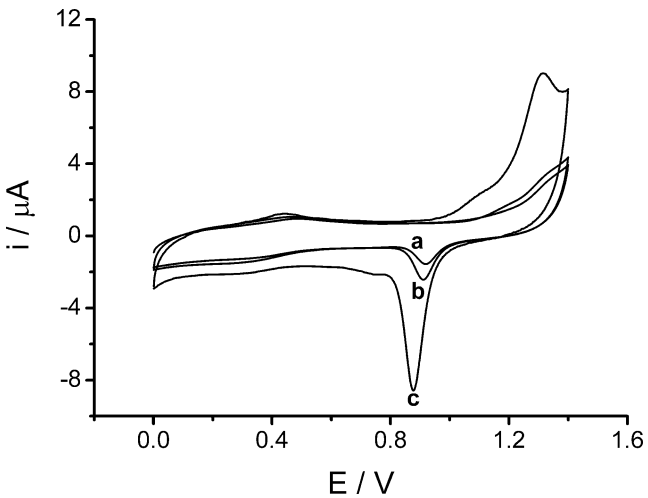

Fig. 3 Cyclic voltammograms of Au–HSM/GCE (**a**), Au–SH–HSM/GCE (**b**), and Au–NH_2–HSM/GCE (**c**) in 0.5 M H_2SO_4; scan rate, 50 mV s^{-1}; geometric area of the electrode surface, 0.033 cm^2

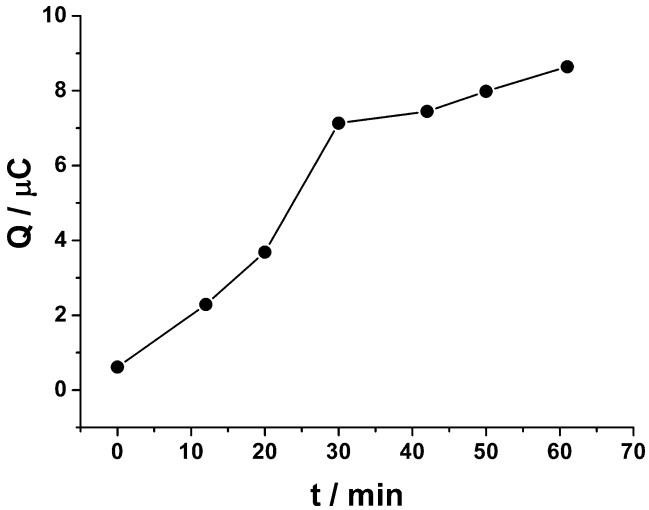

Fig. 4 Influence of immersing time on the integral charge (Q) of the cathodic peak of Au–NH_2–HSM/GCE in 0.5-M H_2SO_4 solution; the geometric area of the electrode surface, 0.033 cm^2

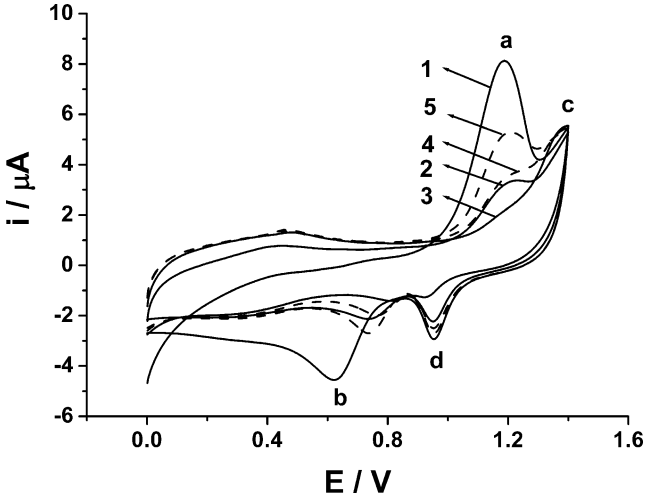

Fig. 5 Cyclic voltammograms of Au–NH_2–HSM/GCE in 0.5-M H_2SO_4. *1* The first cycle scan, *2* the third cycle scan, *3* the 15th cycle scan, *4* as *3* but 1-μl saturated KCl was introduced in the solution, *5* as *3* but 2-μl saturated KCl was introduced in the solution; scan rate, 50 mV s^{-1}; geometric area of the electrode surface, 0.033 cm^2

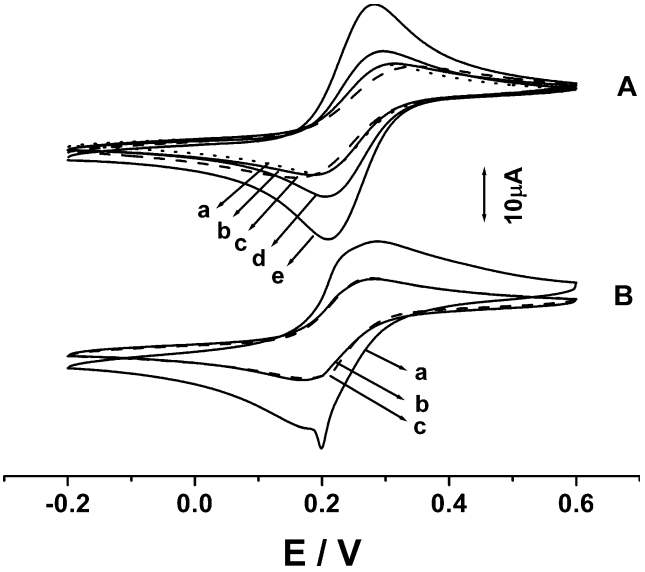

Fig. 6 Cyclic voltammograms of different electrodes in 5-mM $K_3Fe(CN)_6$-1 M KCl solution. Electrodes: HSM/GCE (**a**), SH–HSM/GCE (**b**), PVA/GCE (**c**), NH_2–HSM/GCE (**d**), and bare GCE (**e**) for *A* Au–NH_2–HSM/GCE (**a**), Au–HSM/GCE (**b**), and Au–SH–HSM/GCE (**c**), and for *B* scan rate, 50 mV s^{-1}; geometric area of the electrode surface, 0.033 cm^2

particles. Two couples of redox peaks are observable. With repeating potential scan, peaks a and b decrease and shift in a positive direction. At the same time, peaks c and d increase. After 15 potential scan cycles, the voltammogram no longer changes, and peaks a and b almost disappear. However, peaks a and b appear in the presence of KCl and increase with its concentration rising (Fig. 5). It indicates that peaks a and b result from the redox of Cl^- ions adsorbed on the surface of gold nanoparticles. Peaks c and d should be ascribed to the redox of gold. A similar phenomena was observed when a Ag/AgCl electrode was used as reference electrode, indicating that the adsorbed Cl^- ions comes from $AuCl_4^-$ ions and the SCE.

Voltammograms of $K_3Fe(CN)_6$ on different electrodes

On the NH_2–HSM/GCE, the cathodic and anodic peak currents of $K_3Fe(CN)_6$ increase with the repeating potential scan until achieving a stable value at last, indicating that $[Fe(CN)_6]^{3-/4-}$ ions can be adsorbed on NH_2–HSM films, or/and it takes some time for $[Fe(CN)_6]^{3-/4-}$ ions to achieve a diffusion equilibrium. The adsorbed or/and entrapped $[Fe(CN)_6]^{3-/4-}$ ions can still remain on the NH_2–HSM film after rinsing and immersing in blank solutions for 4 h. However, HSM/GCE and SH–HSM/GCE do not show such phenomenon. The adsorption of $[Fe(CN)_6]^{3-/4-}$ ions on NH_2–HSM/GCE is related to the electrostatic attraction of NH_3^+ groups on the mesoporous silica.

It can be seen in Fig. 6A that the potential differences (ΔE_p) between redox peaks of $K_3Fe(CN)_6$ on the NH_2–HSM/GCE, HSM/GCE, SH–HSM/GCE, PVA/GCE are larger than that on a bare GCE. They are 90, 115, 129, 180 mV (average values of five determinations), respectively. This indicates that the electron transfer rate decreases due to the block of mesoporous silica and PVA composite films. Among them, the ΔE_p for the NH_2–HSM/GCE is smallest. This is related to the adsorption of $[Fe(CN)_6]^{3-/4-}$ ions. As shown in Fig. 6B, the CVs of $K_3Fe(CN)_6$ on Au–HSM/GCE, Au–SH–HSM/GCE, and Au–NH_2–HSM/GCE are unsymmetrical. This phenomenon is more evident for Au–NH_2–HSM/GCE. It can be ascribed to the formation of PB on the surface of gold nanoparticles [24].

EIS of the composite films

Figure 7 shows the EIS of different electrodes in 5 mmol L^{-1} $Fe(CN)_6^{3-/4-}$ solution. The Nyquist plots for all electrodes are a semicircle plus a straight line. But for NH_2–HSM/GCE and Au–NH_2–HSM/GCE, the semicircles are smaller than that of the bare GCE, meaning that these films can reduce the electron transfer resistance to some extent. However, mesoporous silica belongs to an isolating material. Therefore, it can be proposed that the electron transfer reactions can occur within the mesopores [25] and the adsorbed $[Fe(CN)_6]^{3-/4-}$ ions can serve as an electron mediator to facilitate the electron transfer. The semicircle of Au–NH_2–HSM/GCE is larger than that of NH_2–HSM/GCE. This may be due to the deposition of the PB film on the surface of Au–NH_2–HSM.

Formation of PB on gold nanoparticles surface

It is observed that PB film can be deposited on Au–NH_2–HSM/GCE in $K_3Fe(CN)_6$ solution. The more gold nano-

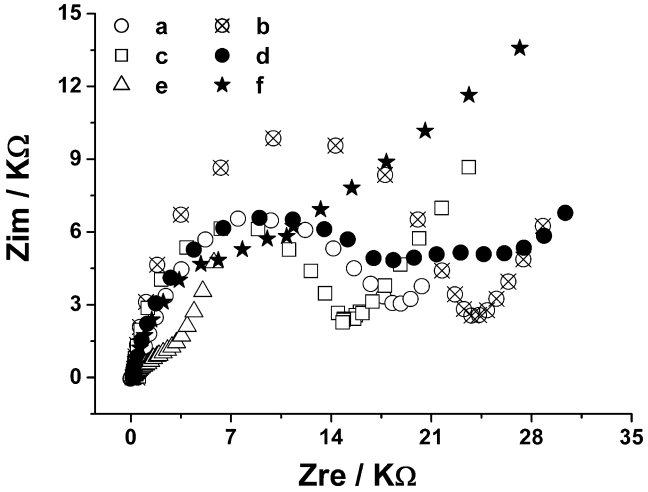

Fig. 7 Impedance spectroscopy of different electrodes. Solution composition, 5-mM $Fe(CN)_6^{3-/4-}$ plus 1-mM KCl and 0.1-M pH 7.0 PBS; electrodes, bare GCE (**a**), HSM/GCE (**b**), SH–HSM/GCE (**c**), PVA/GCE (**d**), NH_2–HSM/GCE (**e**), and Au–NH_2–HSM/GCE (**f**); the frequency range, 100 mHz –100 kHz; the DC potential, 0.25 V (vs SCE); the geometric area of electrode surface, 0.033 cm^2

particles on the NH_2–HSM film electrode, the more PB deposits, meaning that gold nanoparticles can facilitate the formation of PB from single ferricyanide solution. When the successive potential scan number increases, both anodic and cathodic peaks increase until it is up to 15 cycles for Au–NH_2–HSM/GCE (Fig. 8). This indicates that PB is deposited continuously on the electrode surface. Meanwhile, the Au–NH_2–HSM film becomes blue, which further reflects the formation of PB on the electrode surface. The CV of the resulting electrode in K_2SO_4 solution is shown in the inset of Fig. 8. Two couples of well-defined peaks with formal potentials $(E_0 = (E_{pa} + E_{pc})/2)$ of 0.187 V (for peak a) and 0.851 V (for peak b; vs SCE) are observed. The formal potentials are similar to that of the PB-film-modified electrode prepared through usual methods [24, 26–29]. The peaks at 0.187 V corresponds to the following reaction:

$$Fe_4^{III}\left[Fe^{II}(CN)_6\right]_3 + 4e + 4K^+ \rightarrow K_4Fe_4^{II}\left[Fe^{II}(CN)_6\right]_3, \quad (1)$$

whereas the peaks at 0.9 V result from the reaction

$$Fe^{III}\left[Fe^{II}(CN)_6\right]_3 + 3A^- \rightarrow Fe_4^{III}\left[Fe^{III}(CN)_6A^-\right]_3 + 3e, \quad (2)$$

where A^- represents the anion of the supporting electrolyte used. The anodic and cathodic peak currents (i_p) of peaks a and b change linearly with the scan rate (ν) in the range from 10 to 800 mV s^{-1}, indicating that peaks a and b are essentially the surface redox peak.

It should be mentioned that the formation of PB in this case is similar to that reported by Abbaspour and Kamyabi [24]. But in their work, a successive potential scan between −0.2 and 0.6 V (vs Ag/AgCl) cannot lead to PB deposition on an Au electrode surface. PB is obtained only when the potential extends to 0.9 V (vs Ag/AgCl), where ferricyanide ions begin to dissociate. That is to say that the high

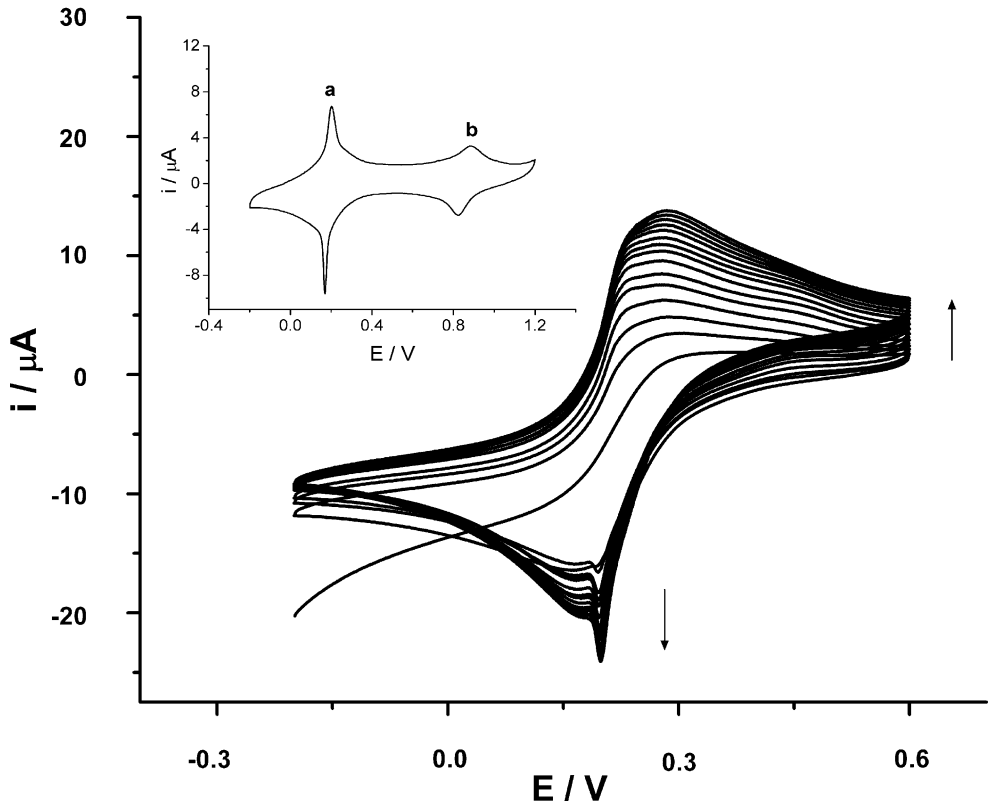

Fig. 8 Successive CV of Au–NH_2–HSM/GCE in 5-mM $K_3Fe(CN)_6$-1 M KCl solution. The inset shows the CV of PB–Au–NH_2–HSM/GCE obtained in 0.25-mM K_2SO_4 solution; scan rate, 50 mV s^{-1}; the geometric area of electrode surface, 0.033 cm^2

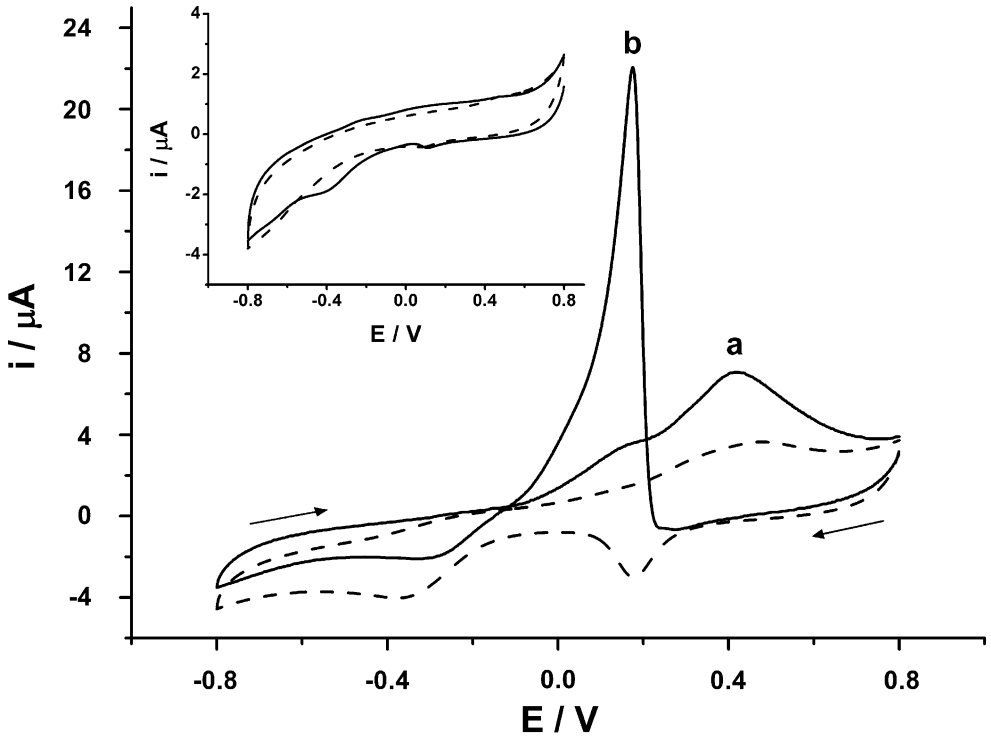

Fig. 9 Cyclic voltammograms of Au–NH_2–HSM/GCE in 0.1-M NaOH solution containing 0 (*dash line*) or 10-mM glucose (*solid line*). The inset shows the corresponding CV on NH_2–HSM/GCE; the geometric area of electrode surface, 0.033 cm^2

potential limit must extend to 0.85 V if a SCE reference electrode is adopted. However, PB can be obtained in the potential range of −0.2 to 0.6 V (vs SCE) in this case. In addition, PB films can be deposited on Au–NH_2–HSM/GCE even using KNO_3 as a supporting electrolyte, which is different from what was reported [24]. The following reasons can account for this phenomenon. Firstly, the strong adsorption of mesoporous silica makes more ferricyanide accumulate on the electrode surface. Secondly, gold nanoparticles have higher catalytic activity than Au electrode that can make the dissociation of ferricyanide ions occur at a lower potential.

Electrocatalytic oxidation of glucose on Au–NH_2–HSM/GCE

Voltammetric response of glucose

The electrocatalytic oxidation of glucose is an attractive topic due to its potential application in developing glucose–oxygen fuel cells and glucose sensor. Thus, it has been studied extensively [30–34]. In this work, the electrocatalytic oxidation of glucose has been studied on Au–NH_2–HSM/GCE. It can be seen in Fig. 9 that glucose exhibits two oxidation peaks on the Au–NH_2–HSM/GCE in 0.1-M NaOH solution, whereas no significant response is observed on NH_2–HSM/GCE. Glucose oxidation occurs at about 0.45 V during the anodic sweep (peak a), which is ascribed to the formation of oxidized glucose intermediate (i.e., gluconolactone); during the cathodic sweep, the oxidation peak occurs at about 0.16 V (peak b), where the gluconolactone is further oxidized to glucose acid [30–33]. The peak b is well defined and more sensitive and is chosen for determination.

As the catalytic oxidation reaction of glucose involves H^+, the solution pH shows marked influences on the peak currents. In neutral and acid solutions, the oxidation peaks of glucose are indiscernible. With the pH rising, peak b increases and shifts in a negative direction. Figure 10 shows the relationship between the peak current of peak b and the OH^- concentration of the supporting electrolyte. When the

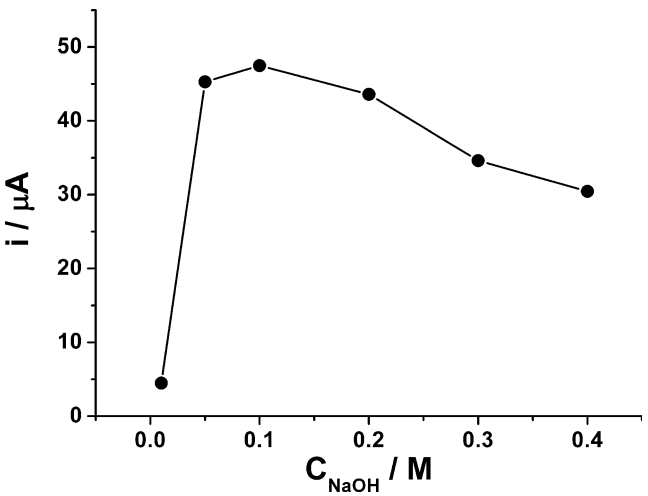

Fig. 10 Influence of NaOH concentration on the peak current of cathodic oxidation peak of 10-mM glucose; the geometric area of electrode surface, 0.033 cm^2

OH^- concentration exceeds 0.1 M, the increase of the peak current slows down. Therefore, 0.1-M NaOH is employed. The effect of OH^- stems from three ways. First, OH^- ion is required to neutralize the proton generated during the dehydrogenation step. Second, the formation of glucose intermediate (gluconolactone) occurs easily in alkaline solution. Third, the formation rate of hydroxyl gold [i.e., $AuOH^{(1-\lambda)}$] catalyst is dependent upon OH^- [33, 34].

Influence of scan rate

It is observed that the peak current (i_p) of peak b of a 10-mM glucose changes linearly with the square root of the scan rate ($\nu^{1/2}$) in the range studied (10–400 mV s^{-1}). The linear regression equation is $i_p(\mu A) = 8.53 + 65.5\,\upsilon^{1/2}\left(V^{1/2}\,s^{-1/2}\right)$ $(R = 0.994)$, indicating that the charge transport through the composite film is apparently diffusion-controlled. Additionally, the peak potential (E_p) shifts in a negative direction with the scan rate growing, and there is a linear relationship between the E_p and ln υ. As for a totally irreversible electrode process, the E_p is defined by the following equation [35]:

$$E_p = E^{0'} + (RT/\alpha nF)\left[0.780 + \ln\left(D_0^{1/2}/K^0\right) + \ln\left(\alpha nF\upsilon/RT\right)^{1/2}\right], \quad (3)$$

where $E^{0'}$ is the formal potential, α is the electron transfer coefficient, n is the number of transfer electron in the rate-determining step, and K^o is the standard heterogeneous rate constant. In this case, E_p and ln υ are consistent with the following equation:

$$E_p = 0.0530 - 0.031\,\ln\upsilon\,(R = 0.976) \quad (4)$$

The slope of $E_p - \ln\nu$ plot indicates that the value of αn_a is 0.41. For an irreversible electrode process, the reasonable α value is usually regarded as 0.5. Supposing that the value of α is 0.5 here, the number of the transfer electron in the electrochemical oxidation can be estimated to be 1. Reversely, the virtual value of α is estimated to be 0.41. This indicates that the peak b can be attributed to the oxidation of gluconolactone to gluconic acid with one electron transfer in the presence of $AuOH^{(1-\lambda)}$ catalyst [33].

Calibration curve and reproducibility

The calibration curve of glucose under the selected conditions is worked out. The peak current is linear to glucose concentration in the range of 0.2 to70 mM, and the linear regression equation is: $I_p(\mu A) = 2.50\,c\,(mM) + 2.35\,(R = 0.999)$. The catalytic current is about 2.5-μA mM^{-1} and the detection limit is 0.1-mM glucose. After each measurement, the modified electrode is regenerated by successively cycling in a 0.5-M H_2SO_4 solution. Through such way an electrode is used to determine a 10-mM glucose for six times and the relative standard deviation (RSD) of the peak current is 3.3%. Five modified electrodes are fabricated to determine a 10-mM glucose and the RSD for the peak current is 9.9%.

Conclusions

Gold nanoparticles can be deposited on NH_2–HSM/GCE by successive potential step method. The diameter of gold nanoparticles obtained is estimated to be about 80 nm. The gold nanoparticles deposited shows high activity. PB films can be deposited on it through cycling potential between −0.2 and 0.6 V (vs SCE) in ferricyanide solution. Au–NH_2–HSM/GCE shows strong catalysis to glucose oxidation in alkaline solution. The cathodic oxidation process of glucose is diffusion controlled and involves one electron transfer. Under the optimized conditions, the cathodic oxidation peak current is linear to the concentration of glucose in the range of 0.2 to 70-mM. The detection limit is estimated to be 0.1-mM. The gold nanoparticles loading mesoporous silica has a potential application in the preparation of glucose–oxygen fuel cell or glucose sensor.

Acknowledgment The authors appreciate the support from the National Nature Science Foundation of China (grant no. 20173040).

References

1. Avgouropoulos G, Ioannides T, Papadopoulou Ch, Batista J, Hocevar S, Matralis HK (2002) Catal Today 75:157
2. Guzman J, Gates BC (2002) J Phys Chem B 106:7659
3. Okumura M, Akita T, Haruta M (2002) Catal Today 74:265
4. Bond GC (2002) Catal Today 72:5
5. Zhou ND, Wang J, Chen T, Yu ZG, Li GX (2006) Anal Chem 78:5227
6. Hrapovic S, Majid E, Liu YL, Male K, Luong JHT (2006) Anal Chem 78:5504
7. Daniel MC, Astruc D (2004) Chem Rev 104:293
8. Welch CM, Compton RG (2006) Anal Bioanal Chem 384:601
9. Fukuoka A, Araki H, Kimura JI, Sakamoto Y, Higuchi T, Sugimoto N, Inagaki S, Ichikawa M (2004) J Mater Chem 14:752
10. Bore MT, Pham HN, Switzer EE, Ward TL, Fukuoka A, Datye AK (2005) J Phys Chem B 109:2873
11. Hagaman EW, Zhu HG, Overbury SH, Dai S (2004) Langmuir 20:9577
12. Gu JL, Xiong LM, Shi JL, Hua ZL, Zhang LX, Li L (2006) J Solid State Chem 179:1060
13. Pérez MD, Otal E, Bilmes SA, Soler-Illia GJAA, Crepaldi EL, Grosso D, Sanchez C (2004) Langmuir 20:6879
14. Ghosh A, Patra CR, Mukherjee P, Sastry M, Kumar R (2003) Microporous Mesoporous Mater 58:201
15. Asefa T, Lennox RB (2005) Chem Mater 17:2481
16. Akolekar DB, Bhargava SK (2005) J Mol Catal A Chem 236:77

17. Aprile C, Abad A, García H, Corma A (2005) J Mater Chem 15:4408
18. Yin BS, Ma HY, Wang SY, Chen SH (2003) J Phys Chem B 107:8898
19. Tanev PT, Chibwe M, Pinnavaia TJ (1994) Nature 368:321
20. Yoshitake H, Yokoi T, Tatsumi T (2003) Chem Mater 15:1713
21. Walcarius A, Etienne M, Sayen S, Lebeau B (2003) Electroanalysis 15:414
22. Li LD, Li WJ, Sun CQ, Li LS (2002) Electroanalysis 14:368
23. Yoshitake H, Yokoi T, Tatsumi T (2002) Chem Mater 14:4603
24. Abbaspour A, Kamyabi MA (2005) J Electroanal Chem 584:117
25. Villemure G, Pinnavaia TJ (1999) Chem Mater 11:789
26. Itaya K, Ataka T, Toshima S (1982) J Am Chem Soc 104:4767
27. Itaya K, Shibayama K, Akahoshi H, Toshima S (1982) J Appl Phys 53:804
28. Itaya K, Uchida I, Toshima S (1983) J Phys Chem 87:105
29. Itaya K, Ataka T, Toshima S, Shinohara T (1982) J Phys Chem 86:2415
30. Larew LA, Johnson DC (1989) J Electroanal Chem 262:167
31. Adzic RR, Hsiao MW, Yeager EB (1989) J Electroanal Chem 260:475
32. Luna AMC, Mele MFLD, Arvia AJ (1992) J Electroanal Chem 323:149
33. Hsiao MW, Adzic RR, Yeager EB (1996) J Electrochem Soc 143:759
34. Cui HF, Ye JS, Liu X, Zhang WD, Sheu FS (2006) Nanotechnology 17:2334
35. Bard AJ, Faulkner LR (2001) Electrochemical methods: fundamentals and applications. Wiley, NY, USA, pp 236